HEURISTIC GENERATION OF MULTISPECTRAL LABELED POINT CLOUD DATASETS FOR DEEP LEARNING MODELS

Lino José Comesaña Cebral*[1], Joaquín Martínez Sánchez[1], Erik Rúa Fernández[1], Pedro Arias Sánchez[1]

[1] CINTECX, Universidade de Vigo. Applied Geotechnology Group, 36310 Vigo, Spain – (linojose.comesana, joaquin.martinez, erik.rua, parias)@uvigo.es

KEY WORDS: Point Cloud, Heuristic Generation, Deep Learning, Road, Forest, Multispectral, Dataset.

ABSTRACT:

Deep Learning (DL) models need big enough datasets for training, especially those that deal with point clouds. Artificial generation of these datasets can complement the real ones by improving the learning rate of DL architectures. Also, Light Detection and Ranging (LiDAR) scanners can be studied by comparing its performing with artificial point clouds. A methodology for simulate LiDAR-based artificial point clouds is presented in this work in order to get train datasets already labelled for DL models. In addition to the geometry design, a spectral simulation will be also performed so that all points in each cloud will have its 3 dimensional coordinates (x, y, z), a label designing which category it belongs to (vegetation, traffic sign, road pavement, …) and an intensity estimator based on physical properties as reflectance.

1. INTRODUCTION

Automatic point cloud labelling to subtract environment features such as trees, road components, … is a challenging task because it does not require hand-crafted features, which are widely used in existing methods like Koppula (2011), Yokoyama (2013) and Song et al. (2014). Point cloud labelling is an important task in computer vision and object recognition (Jing Huang et al., 2016). Depending on the purpose, there are several techniques based on heuristic methods to label each point in a cloud. These methods are designed towards the identification of purely geometrical patterns by the application of different computational settings, such as Machine Learning (Neuville et al., 2021).

With the evolution of Artificial Neural Networks (ANN), more ways to automatic point cloud labelling are appearing nowadays, like Mei et al. (2018) for individual tree subtraction or Balado et al. (2019) for road infrastructure classification. Designing these networks is a challenging task, especially because of the lack of public labelled datasets. In order to avoid this and other expensive solutions, data augmentation by generation of artificial point clouds with label information can improve the ANN's performance.

Complex Deep Learning models requires big datasets during their training. Also, their internal structures can differ depending on the input data type (data source), even if they are designed for the same purpose. Nowadays, there are more public imagery datasets available than LiDAR due to the operational and economic difficulty that presents this last technology employment.

This work shows an algorithm developed for synthetic creation of point cloud datasets of natural environments including roads. Also, for a more realistic scenario, an intensity simulation of a multispectral LiDAR is applied in these point clouds. The scheme that follows this paper is the following: (1) Description of the methodology; (2) Types of environments studied; (3) Geometrical and Spectral designs; and (4) Results and its discussions.

2. METHODOLOGY

2.1 Geometrical design

As mentioned above, the main purpose of this work consists of recreating realistic point clouds in different cases where an Airborne Light Scanner (ALS) or Terrestrial Laser Scanning (TLS) could be used, such as mountain forests or road highways. Following this line, two scenarios are presented: (a) Forest point clouds without any road presence and (b) forest point clouds with road presence. In the second case it is necessary to explain how the road is designed according the Spanish normative.

Independently of the point cloud's type, the first steps of the digital terrain model (DTM) and tree generation are completely common. As will be shown later, once these steps are completed the only remaining part that differs both scenarios are road concerning facts as explained in next subsections.

2.1.1 DTM generation

The first step of this work consists in the simulation of a rough terrain which emulates real mountain grounds. This will be done by setting some curvatures to a previous designed surface.
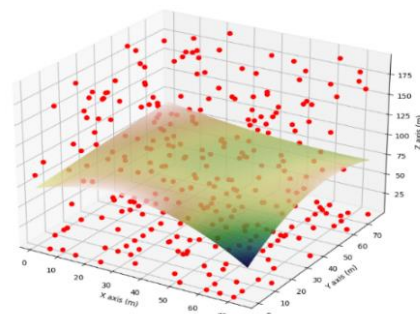

Figure 1. Surface model obtained.

* Corresponding author

First of all, a plane grid of points is defined at a height of $z=0$. After this, some random points are selected and their z coordinates are changed into a random choice from 0 to a maximum height value specified by the user, following a Gaussian-like distribution. Then a 2D quadratic model fit is applied to all points in the cloud (see Figure 1). We chose a quadratic model in order to make a smooth curvature of the terrain, as higher orders cannot always provide. The simulated surface adapts the following expression:

$$\hat{z}(x,y) = a_1 x^2 y^2 + a_2 xy^2 + a_3 y^2 + a_4 x^2 y + \qquad (1),$$
$$+ a_5 x^2 + a_6 xy + a_7 y + a_8 x + a_9$$

where a_i are the quadratic fit parameters. One can rewrite this in terms of its matrix form:

$$\hat{z}(x,y) = G(x,y) \cdot m \qquad (2),$$

where G denotes the variable matrix and m is a vector containing all a_i values.

2.1.2 Road alignment

Once the DTM is generated, the next step consists on the road trajectory simulation. For this purpose, it is necessary to follow some rules concerning to road alignment, like the maximum curvature radius per velocity or the slope angle allowed. The Spanish 3.1-IC normative for road layout (Ley 3.1-IC de Trazado de Carreteras, 2016) will be considered in order to create real-alike roads.

The types of roads that will be created in this works are three: highways, national roads and local roads. Each one of them has its own characteristics as it is reflected in Table 1.

Characteristics	Type		
	Highway	National road	Local road
2 platforms	Yes	No	No
1 platform	Yes	Yes	Yes
Refuge island	Yes	No	No
Lanes	4	2	1-2
Curve radius (m)	250-7500	50-2500	350-3500

Table 1. Some road alignment normatives (Ley 3.1-IC de Trazado de Carreteras, 2016) .

Also, there are more important features as camber angles or signal positioning that can differ depending on environmental and technical parameters such as the shoulder size of the road or the maximum velocity allowed per stretch.

Following these rules, a curve is defined along all points of the surface that fall into its domain. This curve will be the main skeleton of all the infrastructure and all the remaining parts of the
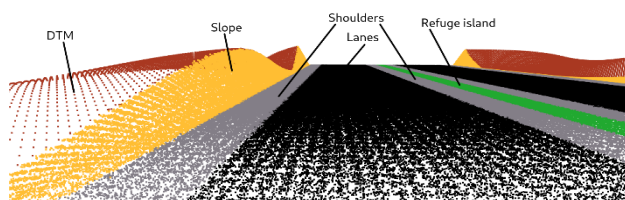
road will be created from the point of view of it. For a clearer view see the graphical design of Figure 2.

In the scenario of a highway type road, the first element that will be created is the refuge island, also known as pedestrian refuge or pedestrian island. In Spanish roads (Ley 3.1-IC de Trazado de Carreteras, 2016), the average size of this element is approximately 2 m, so all points of the surface that fall under a Euclidean distance of $< d_{ri}$ ($d_{ri} = 2$ m) from the previous curve in the XY plane will be grouped as the refuge island set, I. Once all points of I are identified, they are translated into a height z_{road}. After this, knowing that the mean width of the pavement in highway's shoulders is ~2 m, a second set of points S is defined with all points of the surface that fall in a Euclidean distance of $d_{ri} < d < r_{ri} + 2$ m, in the XY plane. As done with the refuge island, all points in S are translated to z_{road}. Lanes are defined in an analogous way following the current normatives (Ley 3.1-IC de Trazado de Carreteras, 2016). The abrupt discontinuity between the shoulders and the DTM is corrected by the definition of a smooth surface that adapts the points of the DTM (in a previously specified buffer) to the outer points of the shoulders. This surface is called slope. The full design can be seen in Figure 2.

If the type of road selected is different, like national and local roads, the methodology exposed in the paragraphs above differs in the creation of the refuge island and in the sizes of the rest parts. A detailed view can be seen in Figure 3.
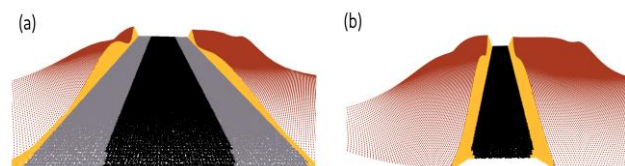

Figure 3. Simplified views of: (a) National road and (b) local road.

2.1.3 Tree filling and signal positioning

Once all road-concerning ground parts are created, the next step consists in placing vegetation and traffic signs on the allowed ground parts.

The best way to get a vegetation set of points is by the employment of an individual tree (IT) segmentation algorithm on real forest point clouds. Depending on the source of measurements, there are a lot of methods in the state of the art, like Zhong et al. (2017), Wang et al. (2021) or Dan Xie, (2020) for TLS point clouds and Lishuo Zhang et al. (2020), Parkan et al. (2015) or Smits et al. (2012) for ALS point clouds. Furthermore, the preferred scenario is that whose points come from a previously combination of ALS and TLS point clouds.

Applying these algorithms provides a new set of vegetation points, V. Now, the DTM surface is filled with different segments of V, depending on the filling degree specified by the user (higher degrees imply more populated DTM's).

Finally, the last part of the geometrical design lies in the creation of traffic signs and barriers. 3D traffic sign models can be designed following the official normatives (Norma 8.1-IC de Señalización Vertical, 2014), or a segmentation method can be applied on a real road point cloud, analogously to the previous vegetation set. Some algorithms are presented in Soilán et al. (2016), Balado et al. (2021) and Wu et al. (2015).

Figure 2. Simplified view of a Highway point cloud and its parts.

Traffic barriers must be created from scratch since the road curve may differs between clouds. The graphical design followed the official Spanish normative (Orden Circular 35/2014 Sobre Criterios De Aplicación De Sistemas De Contención De Vehículos, 2014). Some examples are shown in the Results section.

The main advantage of the geometrical design exposed before is the uncertainty range allowed. Most of the point sets defined before did not came from real point clouds; instead, they were created from scratch following some rules and official normatives. Applying some gaussian noise to each point set in the cloud can provide a scenario were a real scanner performed its measurements (Mei et al., 2018).

Furthermore, considering that these point clouds are created in order to train deep learning models, this uncertainty range, i.e. the deviation degree between these clouds and real ones, can be low enough for achieving a good learning rate in artificial neural networks (ANN) since these models give probability ranges of belonging to the different classes shown before for each set of points (Yuen et al., 2021).

2.2. Intensity simulation

As mentioned at the end of the previous section, the geometrical methodology was exposed in order to create train datasets of deep learning models. For a better performance of these models, an additional dimension can be added to the labelled point clouds, as it is known that ANN's work better with geometrical complex patterns when more features can be learned from them (Abiodun et al., 2018).

In this work an intensity analysis will be done in order to simulate different spectral scanners at different laser wavelengths. With these simulations, ANN's can associate not only the geometrical features to their labels, also they can use the spectral information of each point set for a properly identification of those geometrical patterns learned.

First of all, the main idea of this part consists in recreate a spatial trajectory and in each point of that trajectory the spectral scanner will record all points of the clouds created before inside a predefined range. The spectral analysis of each point is made by the radar equation (Yan et al., 2012):

$$P_r = \frac{\rho}{R^2} 10^{-2Ra/10000} \cos\theta \cdot C \qquad (3),$$

where P_r is the total power received by the scanner, ρ is the spectral reflectance of the target, R is the range of the scanner (distance between scanner and target), a is the atmospheric absorption coefficient in dB/km, θ the incidence angle (i.e. angle between the laser pulse direction and the normal of the target's surface in the impact point) and C is a constant factor related to scanner features, such as the power emitted, the aperture diameter or the power vanished along the scanner volume.

Since C can be assumed as constant in the same experiment, equation (3) can be rewritten as follows:

$$\frac{P_r}{C} = \frac{\rho}{R^2} 10^{-2Ra/10000} \cos\theta \qquad (4),$$

where can be shown that the fraction P_r/C is proportional to the intensity (Kaasalainen et al., 2005). Also, it is known that the height evolution of a is (Höfle et al., 2007):

- Height of 1000 m → a = 0,22 dB/km
- Height of 2000 m → a = 0,17 dB/km
- Height of 3000 m → a = 0,14 dB/km

For ALS clouds, flight heights cannot be very large in order to get the spatial resolutions exposed in the previous section, so the atmospheric absorption approximately does not contributes:

$$\frac{P_r}{C} \approx \frac{\rho}{R^2} \cos\theta \qquad (5).$$

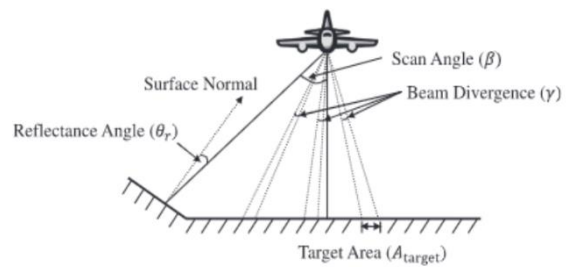Equation (5) shows the quantity that will be computed for each point in the cloud.

Figure 4. Illustration of the reflected angle θ for a laser beam (Yan et al., 2012).

Next step of this simulation procedure consists of the definition of a trajectory suitable for ALS point clouds, for example a grid of points at a predefined height. For the normal estimation of each point in the cloud, Lambertian surfaces are assumed among all sets with adaptive radius. This can be done straightforward with the library Open3D (Zhou et al., 2018). A sketch is shown in Figure 4.

Finally, the spectral reflectance is a quantity that depends on the laser wavelength λ. The Spectral Library of the USGS (Kokaly et al., 2017) contains data of the spectral reflectances measured for different materials in the laboratory, so selecting a laser wavelength in a spectral range can provide the quantity P_r/C and, consequently, an intensity estimator for spectral bands. Examples of the same cloud simulated at different spectral bands are shown in the next section.

3. RESULTS AND DISCUSSION

According to the geometrical and spectral design of the scenarios, some results obtained are shown in this section. First, Figure 5 shows 3 examples of point clouds with highways, since is the most complex scenario as previously explained. Colour schemes of the images in the left side of Figure 5 (a, c, e) correspond to each point class available in highways scenarios i.e. terrain (DTM), vegetation, stony slope, shoulder, lane pavement and refuge island. On the other hand, images in the right side of Figure 5 (b, d, f) were coloured according to the Pr/C values of each point in the cloud.

Analogous, Figure 6 shows 2 examples of point clouds with (a-b) national road and (c-d) forest environment. This last scenario is the simplest since all points in the cloud have the probability of belonging to just two classes: vegetation and terrain (DTM).
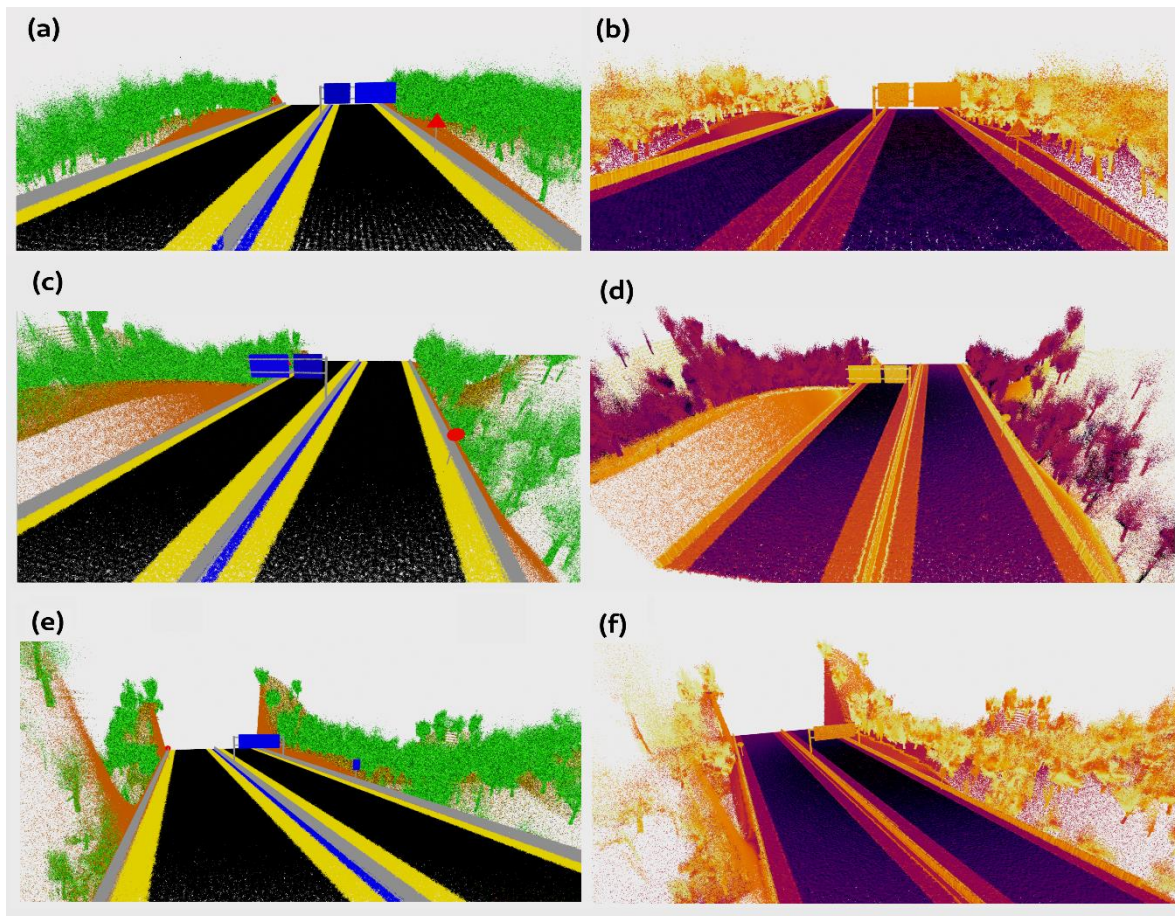

Figure 5. Views of different highway point clouds colored by labels (a ,c ,e) and colored by *Pr/C* values at a laser wavelength of 900 nm (b, d, f).
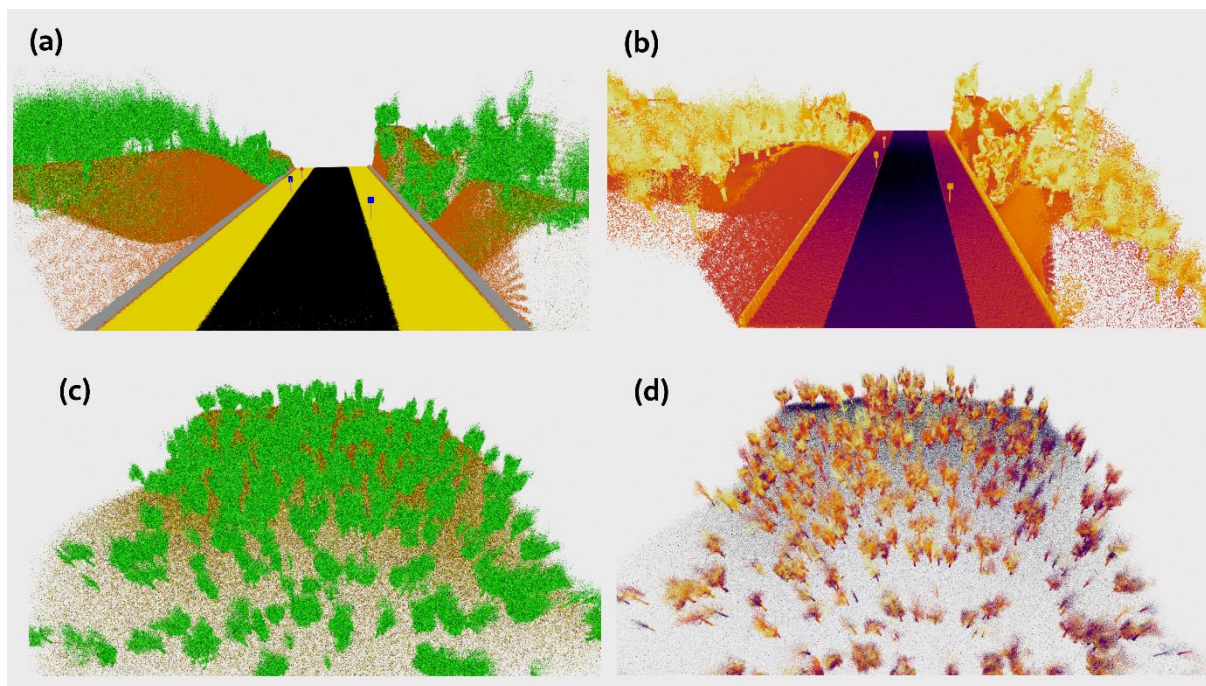

Figure 6. (a,b) Local road point cloud colored by labels and *Pr/C* values at 900 nm of wavelenght and (c,d) generic forest point cloud colored by labels and *Pr/C* values at 900 nm of wavelenght, respectively.
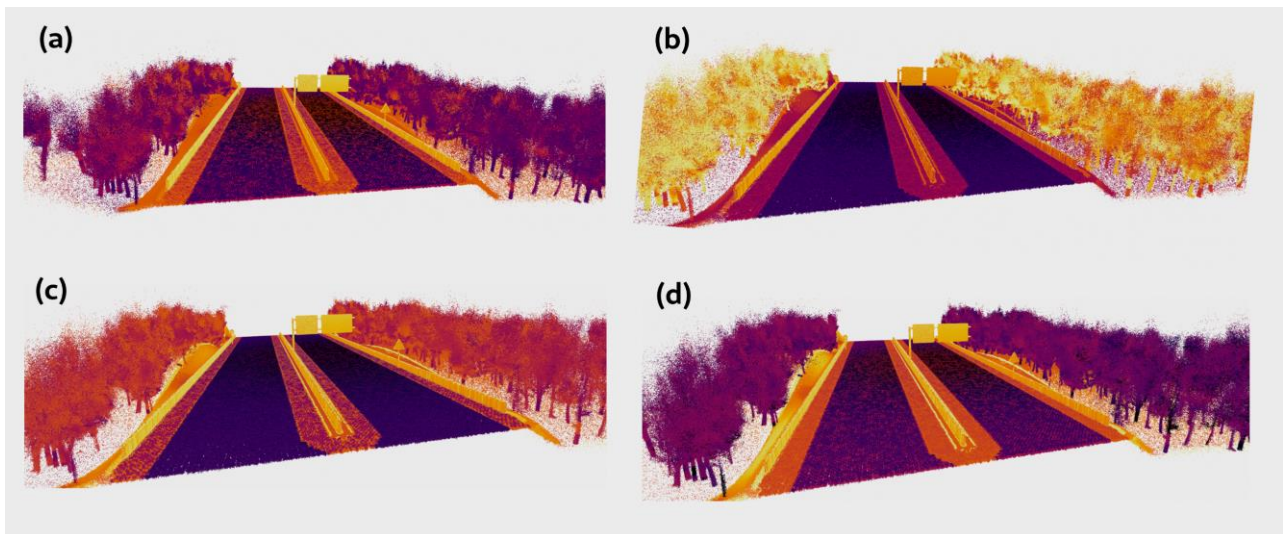
Figure 7. *Pr/C* views of the same highway point cloud at different spectral ranges: (a) 500 nm, (b) 900 nm, (c) 1400 nm and (d) 1928 nm.

4. CONCLUSIONS

Point clouds with multiple labels were created completely from scratch and the results shown in the previous section are very similar to measurements made by a real LiDAR scanner. This similarity is essential and the main key behind the ANN's learning.

The methodology exposed in this work was implemented in a Python program, achieving promising results for further deep learning architectures designs. This tool deals with 4 types of point clouds, and a maximum of 9 class labels per cloud. One way to improve the quality of these clouds is by the definition of more geometries and elements present in road and forest environments (with known reflectances).

Furthermore, the possibility of creating these point clouds in different spectral ranges allow ANNs to associate each geometrical and spectral pattern to the correspondent class label in a more robust way. Combining the results of this method with point clouds taken by real scanners can improve not only ANN's performance but also the development and testing of many segmentation algorithms based on Machine Learning techniques before applying them in real cases.

5. ACKNOWLEDGEMENTS

6. REFERENCES

Abiodun, O. I., Jantan, A., Omolara, A. E., Dada, K. V., Mohamed, N. A., & Arshad, H. (2018). State-of-the-art in artificial neural network applications: A survey. *Heliyon*, *4*(11), e00938. https://doi.org/10.1016/j.heliyon.2018.e00938

Balado, J., Soilán, M., Díaz-Vilariño, L., & van Oosterom, P. (2021). Segmentation Of Traffic Signs From Poles With Mathematical Morphology Applied To Point Clouds. *ISPRS Annals of the Photogrammetry, Remote Sensing and Spatial Information Sciences*, *V-2–2021*, 145–151. https://doi.org/10.5194/isprs-annals-V-2-2021-145-2021

Balado, Martínez-Sánchez, Arias, & Novo. (2019). Road Environment Semantic Segmentation with Deep Learning from MLS Point Cloud Data. *Sensors*, *19*(16), 3466. https://doi.org/10.3390/s19163466

Dan Xie (2020). Individual Tree Segmentation from Terrestrial Laser Scanning Dataset. *2020 Asian Conference on Remote Sensing (ACRS2020)*.

Koppula, H.S., Anand, A., Joachims, T., & Saxena, A. (2011). Semantic labeling of 3d point clouds for indoor scenes. *Advances in Neural Information Processing Systems*, 244–252.

Yokoyama, H., Date, H., Kanai, S., & Takeda, H. (2013). Detection and classification of pole-like objects from mobile laser scanning data of urban environments. *International Journal of CAD/CAM*, *13*(2).

Höfle, B., & Pfeifer, N. (2007). Correction of laser scanning intensity data: Data and model-driven approaches. *ISPRS Journal of Photogrammetry and Remote Sensing*, *62*(6), 415–433. https://doi.org/10.1016/j.isprsjprs.2007.05.008

Jing Huang, & Suya You. (2016). Point cloud labeling using 3D Convolutional Neural Network. *2016 23rd International Conference on Pattern Recognition (ICPR)*, 2670–2675. https://doi.org/10.1109/ICPR.2016.7900038

Kaasalainen, S., Ahokas, E., Hyyppa, J., & Suomalainen, J. (2005). Study of Surface Brightness From Backscattered Laser Intensity: Calibration of Laser Data. *IEEE Geoscience and Remote Sensing Letters*, *2*(3), 255–259. https://doi.org/10.1109/LGRS.2005.850534

Lishuo Zhang, et al. (2020). Comparison of Individual Tree Segmentation based on ALS Point Cloud. *2020 Asian Conference on Remote Sensing (ACRS2020)*.

Mei, L., Zhang, L., Kong, Z., & Li, H. (2018). Noise modeling, evaluation and reduction for the atmospheric lidar technique employing an image sensor. *Optics Communications*, *426*, 463–470. https://doi.org/10.1016/j.optcom.2018.05.072

Norma 8.1-IC de señalización vertical, (2014).

Orden Circular 35/2014 Sobre Criterios De Aplicación De Sistemas De Contención De Vehículos, (2014).

Ley 3.1-IC de trazado de carreteras, (2016).

Neuville, R., Bates, J. S., & Jonard, F. (2021). Estimating Forest Structure from UAV-Mounted LiDAR Point Cloud Using Machine Learning. *Remote Sensing*, *13*(3), 352. https://doi.org/10.3390/rs13030352

Parkan, M., & Tuia, D. (2015). Individual tree segmentation in deciduous forests using geodesic voting. *2015 IEEE International Geoscience and Remote Sensing Symposium (IGARSS)*, 637–640. https://doi.org/10.1109/IGARSS.2015.7325844

Kokaly, R.F., Clark, R.N., Swayze, G.A., Livo, K.E., Hoefen, T.M., Pearson, N.C., Wise, R.A., Benzel, W.M., Lowers, H.A., Driscoll, R.L., and Klein, A.J., 2017, *USGS Spectral Library Version 7* Data: U.S. Geological Survey data release, https://dx.doi.org/10.5066/F7RR1WDJ.

S. Song and J. Xiao. (2014). Sliding shapes for 3d object detection in depth images. *Computer Vision–ECCV 2014*, 634–651.

Smits, I., Prieditis, G., Dagis, S., & Dubrovskis, D. (2012). Individual tree identification using different LIDAR and optical imagery data processing methods. *Biosystems and Information Technology*, *1*(1), 19–24. https://doi.org/10.11592/bit.121103

Soilán, M., Riveiro, B., Martínez-Sánchez, J., & Arias, P. (2016). Traffic sign detection in MLS acquired point clouds for geometric and image-based semantic inventory. *ISPRS Journal of Photogrammetry and Remote Sensing*, *114*, 92–101. https://doi.org/10.1016/j.isprsjprs.2016.01.019

Wang, D., Liang, X., Mofack, G. I., & Martin-Ducup, O. (2021). Individual tree extraction from terrestrial laser scanning data via graph pathing. *Forest Ecosystems*, *8*(1), 67. https://doi.org/10.1186/s40663-021-00340-w

Wu, S., Wen, C., Luo, H., Chen, Y., Wang, C., & Li, J. (2015). Using mobile LiDAR point clouds for traffic sign detection and sign visibility estimation. *2015 IEEE International Geoscience and Remote Sensing Symposium (IGARSS)*, 565–568. https://doi.org/10.1109/IGARSS.2015.7325826

Yan, W. Y., Shaker, A., Habib, A., & Kersting, A. P. (2012). Improving classification accuracy of airborne LiDAR intensity data by geometric calibration and radiometric correction. *ISPRS Journal of Photogrammetry and Remote Sensing*, *67*, 35–44. https://doi.org/10.1016/j.isprsjprs.2011.10.005

Yuen, B., Hoang, M. T., Dong, X., & Lu, T. (2021). Universal activation function for machine learning. *Scientific Reports*, *11*(1), 18757. https://doi.org/10.1038/s41598-021-96723-8

Zhong, L., Cheng, L., Xu, H., Wu, Y., Chen, Y., & Li, M. (2017). Segmentation of Individual Trees From TLS and MLS Data. *IEEE Journal of Selected Topics in Applied Earth Observations and Remote Sensing*, *10*(2), 774–787. https://doi.org/10.1109/JSTARS.2016.2565519

Zhou, Q.-Y., Park, J., & Koltun, V. (2018). *Open3D: A Modern Library for 3D Data Processing*.